Development of an advanced cladding mechanical model and its application for thermal hydraulics coupled failure analysis of SiC LWR fuel cladding during LBLOCA

Hyuntaek Rho, Youho Lee

1, Gwanak-ro, Gwanak-gu, Seoul, Republic of Korea (08826) · Department of nuclear engineering, College of engineering, Seoul National University
*Corresponding author: leeyouho@snu.ac.kr

1. Introduction

In recent years, research on Accident Tolerant Fuel (ATF) cladding that can maintain performance with improved tolerance even in serious accident situations has been actively conducted. As one such ATF candidate, SiC fiber reinforced cladding has been studied a lot. SiC has a melting point of 2730°C and maintains strength even at high temperature of 1500°C [1]. SiC is chemically stable and has four orders of magnitude lower corrosion rate than zircaloy for steam at high temperatures [2]. These characteristics are expected to have strengths in accident situations such as large break loss of coolant accident (LBLOCA) [3]. Although phenomena such as thermal conductivity degradation and swelling occur due to radiation damage, these effects were found to saturate at the operating temperature of the LWR [4]. Despite these strengths, SiC cladding is still in the concept development stage with several drawbacks.

As materials for nuclear grade SiC cladding, Chemical Vapor Deposited (CVD) monolithic SiC (mSiC) and Chemical Vapor Infiltration (CVI) SiC$_f$/SiC Ceramic Matrix Composite (CMC) are used. CVD-SiC cannot be used alone for cladding because it has brittle nature due to the characteristics of ceramics and shows statistical failure behavior. Therefore, it is necessary to use CVI SiC$_f$/SiC with pseudo-ductility to compensate for this. By combining the two, a triple-layer structure consisting of an inner mSiC layer, a middle CMC layer, and a monolithic environmental barrier coating (EBC), or a double layer structure consisting of an inner CMC layer and an outer mSiC layer is studied as a multi-layered SiC cladding. In addition, when SiC is irradiated, swelling occurs. These features are the parts that SiC cladding is fundamentally different from zircaloy, and a specialized model is needed to analyze them.

In this study, a model that can calculate the stress distribution at full rod scale using Finite Difference Method (FDM) was developed, and comparative verification with Finite Element Analysis (FEA) ANSYS code was completed.

The stress distribution of double layer and full SiC$_f$/SiC composite cladding in normal operation, shutdown and LBLOCA conditions was analyzed through linkage with the MARS code, a thermal hydraulic code developed by Korea Atomic Energy Research Institute (KAERI). Based on this, highly probable failure scenarios of duplex SiC cladding and full SiC$_f$/SiC composite cladding in an accident situation are presented.

2. Modeling

2.1 Derivation of displacement formulation

The primary goal is to express the equilibrium equations (Eq. (4) and Eq. (5)) as radial displacement (u_r) and axial displacement (u_z) using the constitutive equations and deformation relations. This is called displacement formulation.

For this, the stress field is expressed as the strain field and then the strain field is expressed as the displacement field.

Equilibrium equations for stress in the axisymmetric cylindrical coordinate system are presented in Eqs.(1)-(2).

$$\frac{\partial \sigma_{rr}}{\partial r} + \frac{\partial \tau_{rz}}{\partial z} + \frac{\sigma_{rr} - \sigma_{\theta\theta}}{r} = 0 \tag{1}$$

$$\frac{\partial \sigma_{zz}}{\partial z} + \frac{\partial \tau_{rz}}{\partial r} + \frac{\tau_{rz}}{r} = 0 \tag{2}$$

Constitutive equations for stress and strain in the elastic region are given by Eqs. (3)-(6).

$$\epsilon_{rr} = \frac{\sigma_{rr}}{E_{rr}} - \frac{V_{\theta r}\sigma_{\theta\theta}}{E_{\theta\theta}} - \frac{V_{zr}\sigma_{zz}}{E_{zz}} + \alpha_{rr}\Delta T + S_{rr} \tag{3}$$

$$\epsilon_{\theta\theta} = \frac{\sigma_{\theta\theta}}{E_{\theta\theta}} - \frac{V_{z\theta}\sigma_{zz}}{E_{zz}} - \frac{V_{r\theta}\sigma_{rr}}{E_{rr}} + \alpha_{\theta\theta}\Delta T + S_{\theta\theta} \tag{4}$$

$$\epsilon_{zz} = \frac{\sigma_{zz}}{E_{zz}} - \frac{V_{rz}\sigma_{rr}}{E_{rr}} - \frac{V_{\theta z}\sigma_{\theta\theta}}{E_{\theta\theta}} + \alpha_{zz}\Delta T + S_{zz} \tag{5}$$

$$\gamma_{rz} = \frac{\tau_{rz}}{G} \tag{6}$$

Where E is Young's modulus, ν is Poisson's ratio, α is coefficient of thermal expansion, G is shear modulus, S is swelling induced strain.

In the cylindrical coordinate system, the deformation relation between strain and displacement is as shown in Eqs. (7)-(10) in the case of axisymmetric cylinder.

$$\epsilon_{rr} = \frac{\partial u_r}{\partial r} \tag{7}$$

$$\epsilon_{\theta\theta} = \frac{u_r}{r} \tag{8}$$

$$\epsilon_{zz} = \frac{\partial u_z}{\partial z} \tag{9}$$

$$\gamma_{rz} = \frac{\partial u_r}{\partial z} + \frac{\partial u_z}{\partial r} \tag{10}$$

After changing the equilibrium equation (Eq. (1) and Eq. (2)) into an equation having u_r and u_z as variables, it becomes the second-order partial differential equation. The equation can be differentiated using FDM.

2.2 Differentiate by applying the FDM

In the modeling of this study, FDM was numerically analyzed using MATLAB. FDM has the advantage of fast computation. In particular, considering the characteristics of the cladding that the mesh shape is simple and the height is too long for the thickness, the analysis using FDM is a method that can achieve high accuracy and speed.

When applying FDM, it should be noted that central differentiation should be used in the inner meshes (5 in Fig. 1.(b).), and forward or backward differentiation should be used in the boundary meshes (1,2,3,4,6,7,8,9 in Fig. 1.(b).) depending on the position.

2.3 Boundary conditions

For the boundary meshes, various boundary conditions must be satisfied in addition to the equilibrium equation.

When hydraulic pressure is applied to the surface, the stress is always applied in a direction perpendicular to the surface. Therefore, since there is no shear stress on the boundary meshes, $\tau_{rz} = 0$.

The pressures applied to the inner and outer walls are P_i and P_o, respectively. By Saint-Venant's principle, the stress at the end cap is $\frac{P_i r_i^2 - P_o r_o^2}{r_o^2 - r_i^2}$.

It can be seen that the bottom surface of the cladding is fixed to the ground. That is, the displacement in the axial direction from the bottom surface can be set to zero. This is physically rational, and by introducing this boundary condition, it is possible to set a reference point for axial displacement.

These boundary conditions are summarized in Fig. 1 and Table I.
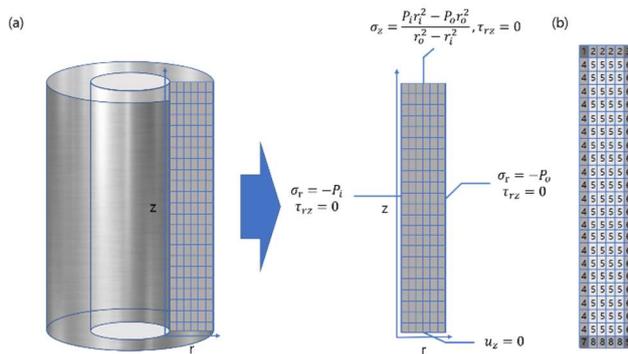
Fig. 1. (a) Boundary conditions of the axisymmetric cladding model, (b) mesh division for differentiation

Table I: Boundary conditions of cladding

Boundary	Boundary condition
Inner surface	$\sigma_r = P_i, \tau_{rz} = 0$
Outer surface	$\sigma_r = P_o, \tau_{rz} = 0$
Cap surface	$\sigma_z = \frac{P_i r_i^2 - P_o r_o^2}{r_o^2 - r_i^2}, \tau_{rz} = 0$
Bottom surface	$u_z = 0$

2.4 Comparative verification with ANSYS in duplex cladding model

Fig. 2 is a graph comparing the results of calculating the stress distributions in the radial, hoop, and axial directions when the temperature distribution is given in the radial direction in a cladding made of two materials (CVD SiC and SiC$_f$/SiC) to the results of ANSYS codes using FEM. Material properties used in simulation are summarized in Table II.

It should be noted that the code used in this study was able to derive accurate results without introducing additional boundary conditions for stress or strain at the interface. By simply assigning different material properties for each location, it was possible to derive an accurate calculation.

Table II: Material properties of CVD SiC and SiC$_f$/SiC used in simulation

Materials	Young's modulus (GPa)	Poisson's ratio	Thermal conductivity (W/m·K)	Thermal expansion coefficient (1/K)
CVD SiC	460	0.21	22.6	4.6×10^{-6}
SiC$_f$/SiC	200	0.3	30	1.2×10^{-5}
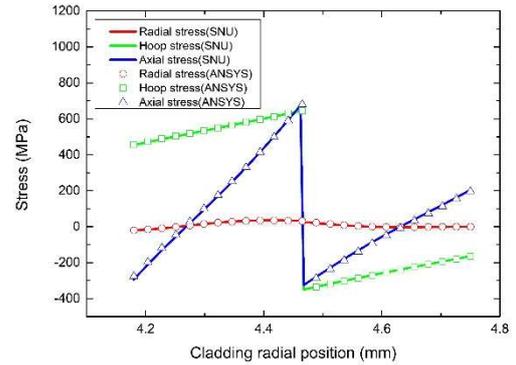
Fig. 2. Comparison of the developed model with finite element analysis solution by ANSYS: cladding thickness = 0.57 mm (CVD SiC : SiC$_f$/SiC = 5:5), $q' = 18$ kW/m, $T_o = 340\,℃, T_{ref} = 22\,℃, P_i = 20$ MPa , $P_o = 1$ MPa.

3. Pseudo-ductility

Unlike conventional ceramic or metallic materials, CMC has pseudo-ductility [5]. Before the load exceeds the proportional limit stress (PLS), the load is distributed to the matrix and fiber, and linear elastic behavior is shown. When a load exceeding the PLS is applied, the matrix and the fibers undergo cracks, resulting in pseudo-ductile behavior due to fiber realignment and slippage. As shown in Fig. 3, when unloaded after PLS, it returns to the original shape without any noticeable offset strain (red path). When reloaded, the stress increases with the decreased Young's modulus (green path). As such, the effective young's modulus (E$_{eff}$) changes depending on the stress, and failure occurs when the ultimate tensile stress (UTS) is reached (purple path).

Therefore, Young's modulus is determined according to the stress history of CMC.
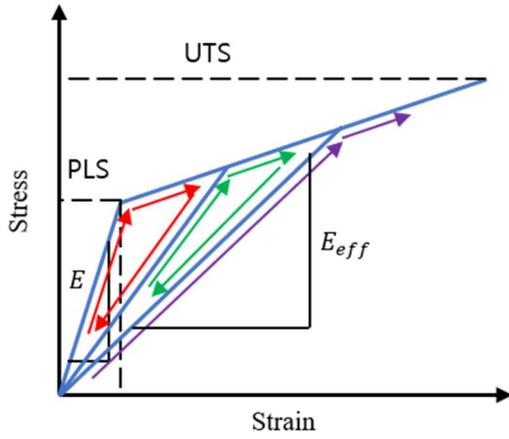
Fig. 3. Pseudo-ductile stress-strain curve

In order to simulate the pseudo-ductile behavior of CMC, the E_{eff} was changed according to the applied maximum stress and E_{eff} were matched in the given stress-strain curve through iteration.

Fig. 4 is a simulation of a situation in which a strong tensile stress is applied to the inside of the full SiC_f/SiC composite cladding due to swelling in the shutdown. In the case of the model without introducing pseudo-ductility, the hoop stress at the inner wall increased to 400 MPa, close to the UTS. In the model to which pseudo-ductility was applied, it was confirmed that Young's modulus and stress rapidly decreased when a stress higher than PLS was applied. Using this model, it is possible to observe the matrix cracking propagation. This is indicated by the white dotted line in Fig. 4.
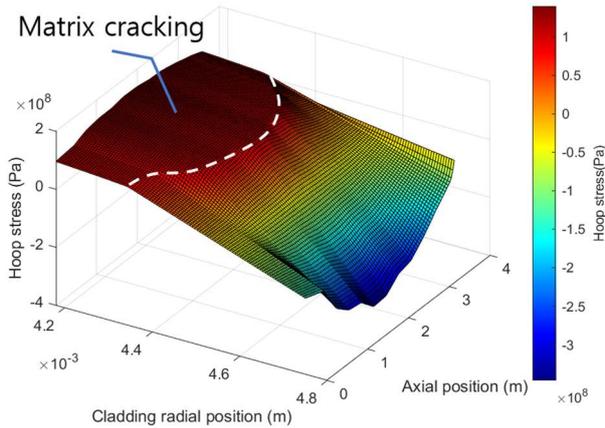
Fig. 4. Stress distribution of full SiC_f/SiC cladding in shutdown situation considering pseudo-ductility

4. Results and Discussion

4.1 Normal operation (End of life)

The material properties of SiC change when irradiated, but tend to converge at a small irradiation dose [4]. Fig.

5 is a contour showing the stress profile and overall stress distribution caused by swelling, thermal expansion, and pressure at the mid-rod location in duplex and full composite cladding.
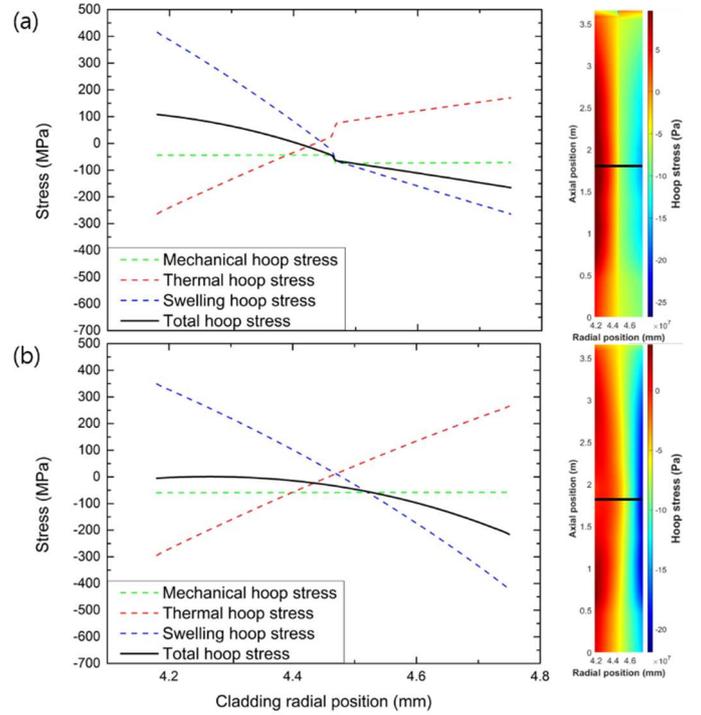
Fig. 5. Stress distribution of (a) duplex cladding (b) full SiC_f/SiC cladding in EOL

From Fig. 5.(a), it can be seen that the outer mSiC layer is under compressive stress. Since CVD SiC shows much stronger strength under compressive stress than in tensile stress, it can be seen that the duplex structure is structurally stable.

Even in composite, it was confirmed that low tensile stress or compressive stress was applied at all locations.

4.1 LBLOCA simulation

LBLOCA simulation was carried out in conjunction with the thermal hydraulic code MARS. Fig. 6.(a) shows the change of boiling mode by cladding axial position, depending on the elapsed time of the accident.

In the event of an accident, a large tensile stress is applied to the mSiC layer in the duplex. The failure of mSiC is defined as Eq. (11) by Weibull weakest link theory.

$$P_f(V) = 1 - \exp\left[-\frac{1}{V_0}\int_V\left[\left(\frac{\sigma_\theta}{\sigma_0}\right)^m + \left(\frac{\sigma_z}{\sigma_0}\right)^m\right]dV\right] \quad (11)$$

Based on this, the result of calculating the failure probability of mSiC according to the accident progress time is shown in Fig. 6.(b). It can be seen that the failure probability reaches 1 after the refill period.

Even in an accident situation, thanks to the pseudo-ductility, it was possible to obtain the result that the stress was not applied enough to destroy the composite and the coolable geometry could be maintained. However, depending on the propagation thickness of matrix cracking, there is a possibility that the fission products may leak to the outside. Therefore, the maximum propagation depth of matrix cracking is shown for each structure in Fig. 6.(c).
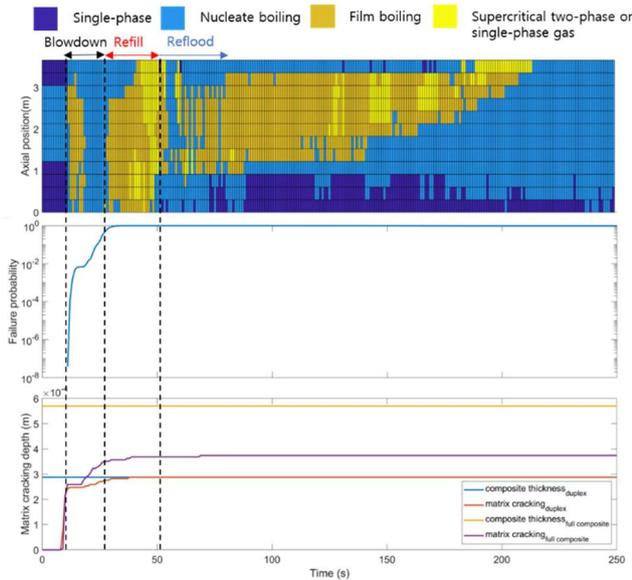
Fig. 6. (a) boiling mode, (b) failure probability of mSiC in duplex structure, and (c) matrix cracking depth depending on the elapsed time of the accident.

As shown in Fig. 6.(c), in the duplex structure, matrix crack propagated as much as the thickness of the composite. However, in full SiC$_f$/SiC composite cladding, about half of the thickness is in a state where cracks are not propagated. Therefore, it seems to be able to maintain hermeticity.
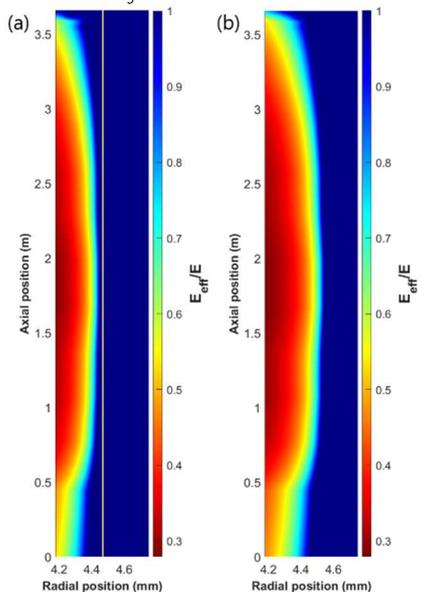
Fig. 7. Young's modulus decrease in (a) duplex and (b) full SiC$_f$/SiC composite cladding at the end of the accident

Fig. 7 shows ratio of E_{eff} and original Young's modulus according to the location in duplex and full SiC$_f$/SiC composite cladding at the end of the accident.

4. Conclusions

A multi-dimensional cladding structure analysis code was developed using FDM. The developed code was applied to SiC cladding, which is attracting attention as ATF. In conjunction with the thermal hydraulic code, MARS, the stress distribution was calculated for the duplex structure and the full SiC$_f$/SiC composite structure under normal operating conditions, shutdown, and LBLOCA conditions.

The pseudo-ductility, a characteristic of SiC composite that ceramic or metal does not have, was introduced into the model. As a result of applying pseudo-ductility, it was found that the composite was not destroyed even in extreme situations such as shutdown or LBLOCA.

In the duplex structure, the outer mSiC layer has a high failure probability due to tensile stress during an accident. Considering that the propagation of matrix cracking occurs as much as the thickness of the layer in the inner CMC layer, it seems that the coolable geometry can be maintained but the hermeticity cannot be maintained.

On the other hand, in full SiCf/SiC composite cladding, matrix cracking propagated less than the thickness while showing low stress distribution due to pseudo-ductility. And because the outside is subjected to a weak compressive stress, it seems that the propagation of matrix cracking can be effectively restrained. Therefore, it seems that both coolable geometry and hermeticity can be maintained.

REFERENCES

[1] Snead, L. L., Nozawa, T., Katoh, Y., Byun, T. S., Kondo, S., & Petti, D. A. (2007). Handbook of SiC properties for fuel performance modeling. Journal of nuclear materials, 371(1-3), 329-377.
[2] Lee, Y. (2013). Safety of light water reactor fuel with silicon carbide cladding (Doctoral dissertation, MIT).
[3] Lee, Y., McKrell, T. J., Yue, C., & Kazimi, M. S. (2013). Safety assessment of SiC cladding oxidation under loss-of-coolant accident conditions in light water reactors. Nuclear Technology, 183(2), 210-227.
[4] Koyanagi, T., Katoh, Y., Singh, G., & Snead, M. (2017). SiC/SiC cladding materials properties handbook. ORNL/TM-2017/385, Oakridge National Laboratory.
[5] Katoh, Y., Ozawa, K., Shih, C., Nozawa, T., Shinavski, R. J., Hasegawa, A., & Snead, L. L. (2014). Continuous SiC fiber, CVI SiC matrix composites for nuclear applications: Properties and irradiation effects. Journal of Nuclear Materials, 448(1-3), 448-476.